The International Journal of Advanced Manufacturing Technology (2018) 97:3711–3721
https://doi.org/10.1007/s00170-018-2173-9

ORIGINAL ARTICLE

A robust and accurate automated registration method for turbine blade precision metrology

Wantao He[1] · Zhongwei Li[1] · Yanyan Guo[1] · Xu Cheng[1] · Kai Zhong[1] · Yusheng Shi[1]

Received: 9 August 2017 / Accepted: 13 May 2018 / Published online: 29 May 2018

Abstract
Turbine blades with complex features are a critical part of turbomachinery, and the manufacture of geometric dimensions and tolerances is strictly controlled to ensure the efficiency and safety of the engines. Precision inspection under current industry practices is challenging and inefficient; however, inspection with an optical device is a promising technique. One key task involved is registration that aligns the measurements to the part model to achieve a fast and automatic inspection process. We present robust and accurate coarse and fine automated registration methods for turbine blade precision metrology. An iterative scan strategy is used to obtain sufficient point clouds to construct curves and surfaces using a B-spline method for registration. Then, principal axes of the reconstruction surface of the blade are calculated, and a principal component analysis (PCA)-based coarse registration method is used. The coarse alignment of the measurement data and the computer-aided design (CAD) model are optimized by fine registration using a common iterative closest point (ICP) algorithm. In this step, the signal-to-noise ratio is incorporated in the transformation of correspondence sets to reduce or remove the noise of outliers. These techniques have been implemented in a four-axis blade inspection system with a point-based conoscopic holography sensor. The results of measurement simulation experiments and inspection case studies indicate that the presented registration method is robust and accurate.

Keywords Turbine blade · Optical inspection · Coarse and fine registration · ICP algorithm · Free-form surface · Four-axis inspection system

1 Introduction

Blades with a free-form surface and strong twist are key components that are used in several important industries, such as aviation engines, steam turbine generators, and automatic transmissions. To ensure that these turbine engines operate efficiently and safely, the geometric dimensions and tolerances of blades must be strictly controlled. Blade shapes are typically measured using three methods: dedicated hard gauges, coordinate measurement machines (CMMs), and optical non-contact inspection systems [1–3]. The use of fixed and functional gauges to measure blades is straightforward and fast; however, many gauges are required, and they occupy inventory space and require regular maintenance, calibration, and repair for accuracy. The technique of removal and replacement of dedicated hard gauges with faster measurement tools is becoming increasingly achievable [4]. A CMM is essentially a Cartesian robot with one tactile probe. While the CMM measures the parts with high precision, a conventional tactile probe is often limited in scanning speed, and the probe radius compensation direction is prone to error in the measurement of tiny objects. The tactile probe is particularly cumbersome when measuring blades with complex free-form 3D geometry shapes because maintaining continuous contact with the surfaces is challenging. Large errors can arise during the manufacturing procedure due to the geometrical complexity (i.e., the cosine error) [5]. Mansour G

✉ Zhongwei Li
zwli@hust.edu.cn

Wantao He
wantaohe@hust.edu.cn

[1] State Key Laboratory of Material Processing and Die and Mould Technology, Huazhong University of Science and Technology, Wuhan 430074, China

[6] used polynomials and third-order curves to find the minimum number of points required for the dimensional control of a blade in a CMM machine; the test time was reduced dramatically. Because of the incorrect results caused by significant variations in the shape of the blade, particularly near the upper sections, the leading edge, and the trailing edge, a two-step measurement procedure of the blade shape and an analysis technique has been proposed to improve the accuracy [7]. Although blade profile inspection using CMM methods has reached a certain level of sophistication, the accuracy (particularly in the leading and trailing edge) and speed can still be improved. If we wish to inspect a blade in three dimensions for repair service and reverse engineering, the measurement speed of CMM is unacceptably low. In these cases, 3D non-contact optical inspection systems, including structured light (laser triangulation and white light fringe projection), interferometry (conoscopic holography and white light interferometry), and focus variation methods, are becoming more capable and affordable for the rapid acquisition of surface shapes [8]. Among non-contact methods, the point-based range sensors have the highest precision and are particularly appropriate for blade measurement. One of the drawbacks of high-precision point sensors is that they have a limited working range. The highest accuracy is achieved when the measurement surface lies at the center of the working range. Therefore, the measurement path must be planned [9]. To accurately translate the plan from the computer-aided design (CAD) model to the machine, one of the most challenging problems is to develop a robust and accurate registration method that aligns the measurement coordinate system (MCS) and the CAD/part coordinate system (PCS). Registration methods can be classified into fixture-based registration, the traditional 3-2-1 approach to registration, and geometry-based registration [10–13]. For quick alignment during the measurement process, industry practices often adopt a high-precision fixture with a plane or certain features manufactured according to the part to determine the part orientation. Using this method, finding the homogeneous transformation matrix between the MCS and the PCS system is relatively straightforward. The orientation accuracy is clearly affected by the assembly tolerance between the fixture and the part; more importantly, a fixture with precise dimensions can be challenging to manufacture and requires regular maintenance or is not available in certain cases. The 3-2-1 approach is a general method for free-form part inspection using the touch probe CMM. The method relies on the skill of the operator, and the speed is slow because several iterations are often necessary to measure points at the exact location as the corresponding points on the CAD model. The above two methods require manual involvement and cannot be automated. Geometry-based registration can be automated to align the multi-view point clouds from one sensor or multiple sensors in computer graphics. However, many of these approaches aim to align complex shapes that have abundant features for which accuracy is not critical. This approach is not robust for turbine-blade high-precision inspection and automation. We present a robust and accurate algorithm to align smooth free-form surfaces for the automated precision metrology of turbine blades.

The rest of the paper is structured as follows. Section 2 reviews and discusses available registration methods. Based on these methods and their analysis, a new geometry-based registration method is presented in Section 3. Section 4 introduces a four-axis optical inspection system incorporated with the implemented registration method. Finally, the conclusions are summarized in Section 5.

2 Review of related work

An inspection methodology consists of inspection planning and post-processing steps. Registration is a key issue in the two steps. The efficiency of measurement planning is directly affected by robust registration. The registration accuracy directly determines whether the error analysis, which calculates deviations of measurements from the nominal CAD model, is accurate. The geometry-based registration process consists of several steps, as shown in Fig. 1. The process can be divided into two steps: coarse and fine registrations (matching or location). The coarse registration roughly aligns the dataset in the first step, which is the most important part of the registration process because the result affects fine registration. Fine registration is generally formulated as an optimization problem involving the search for motion parameters (three rotation angles and a translation vector) that are as accurate as possible [14]. However, the convergence domains of the optimization processes are small, and a satisfactory initial guess is required; otherwise, false matching solutions will be obtained. Various techniques have been developed to supply coarse registration to obtain a good initial guess. Coarse registration can be further divided into three different steps: detection, description, and searching strategies [15].

If the measured surface includes certain distinctive geometry elements such as holes, slots, or pockets, these features can be adopted to align the CAD model and the measurement data to obtain coarse registration [16]. However, most measured parts (e.g., blades) with smooth free-form surfaces do not contain any geometric characteristics. These methods are not particularly suitable in such cases. Some local feature descriptors are defined, such as the spin image [17], point signature [18], and surface signature [19]. Those descriptors are popular representations for image registration in computer vision. A spin image is created as a local 2D image for each chosen oriented point by recording the distances to the fitted

Fig. 1 Registration pipeline

plane and to the normal vector of the neighborhood point. The point signature is defined as a distance profile circulated around the point and is thus invariant to the part orientation. If the signatures of two separate points from the measurement and the part model are matched within the tolerance band, then a correspondence pair is found. These methods typically deconstruct the 3D information of the surface into a stack of 2D descriptors to which robust 2D image matching techniques can be applied. These methods are effective and robust to match free-form surfaces. However, the measured surfaces in precision engineering are normally smooth, and local shape variations are negligible. The spin image and point signature method may lead to false correspondences because there is little geometrical information included in each signature. Therefore, these methods are not appropriate for application in precision engineering.

In the field of precise measurement, researchers have used simple features on the surfaces to align the point cloud and the CAD model for coarse registration. A five-feature-point prefixture method is proposed in Refs. [20, 21]. The gravity center and four corner points are defined for each surface as characteristic points. The four corner points that are farthest from gravity in the measured surface are defined to obtain the largest envelop area. Then, the measurement surface is rotated to minimize the sum of the distances between the five characteristic point pairs. The method assumes that the measurement surface and the CAD model are of the same size and approximately from the same location. The precision inspection registration process for measurement planning typically measures one small region of the part to match the CAD model; thus, global features such as the gravity center or normal vectors will be invalid. Certain other 3D features were studied in Ref. [22]. A surface feature is defined based on surface differential geometric shapes, which include concave, convex, saddle, and flat, using the internal and external attributes of a feature to perform surface coarse matching. This method is not suitable for blade measurement registration because the surface of a blade has only concave or convex geometric features on one side, resulting in a lack of external attributes. Based on the point signature [18], a novel generalized feature named the structured region signature (SRS) was presented in Ref. [23], The SRS is a 2D signal extracted by cutting the surface with a sphere; this signature can make the best use of the shape information in the signature curves, and a more reliable matching result can be obtained in coarse registration. However, this method does not consider noise or outlier influence. An invariant feature-pattern-based form characterization (IFPFC) method is presented by Ref. [24]. It makes use of intrinsic surface features to map the surface into an orientation-independent feature pattern to represent the surface geometry. Compared with other methods, the IFPFC is robust and efficient.

When a close initial configuration is supplied by the coarse matching, fine registration will be conducted to obtain relatively high matching accuracy. The iterative closest point (ICP) algorithm presented by Ref. [25] is the most widely used final optimization method. This method iteratively calculates the optimal transformation parameters to minimize the distances between the measurement points and the CAD model. There are many limitations of the ICP method: it is time-consuming to calculate the closest-point correspondences, false correspondences often appear and are not straightforward to distinguish, and the iterative process tends to be trapped at a local minimum. Therefore, various methods and heuristics have been proposed to improve the efficiency, accuracy, and robustness of the ICP algorithm at its different stages. Ref. [26] presented an optimized ICP algorithm that uses a constant-time variant for finding point pairs and compared the convergence speed of several ICP variants. The results showed that point-to-plane correspondence has a faster convergence rate than point-to-point correspondence. Ref. [27] constructed an efficient ICP algorithm for free-form surface precision inspection by combining various techniques. However, how to obtain the initial pose was not addressed in detail. To meet the sub-micrometer level of accurate assessments in dimensional metrology, three ICP variants were proposed in Ref. [16]. To increase robustness, generalized-ICP [28] and sparse-ICP [29] methods have been presented.

In summary, the ICP algorithm can register several types of geometric data, such as point sets, triangle sets, implicit surfaces, or parametric surfaces, and the algorithm is straightforward to implement with multiple possible speeds and robustness enhancements. If a fair initial orientation is provided, the algorithm still provides the most accurate registration results by far in the application of precision inspection. The next section presents a robust and accurate algorithm for blade automation registration using the ICP method.

3 The registration method for blade precision measurement

Measurement path planning is required for high-precision point sensors to maintain a constant standoff with the part's surface in the measurement process. To accurately translate the plan from the CAD model to the machine, a robust and

high-precision registration method is required. Unlike traditional industrial components and simple geometries, most blade surfaces have no salient features or shape parameters for use with matching and alignment. To achieve the reliable registration of measured data and the CAD model, a two-step registration method is adopted. A novel coarse registration method is presented to make the measurements with a small deviation range; then, precision alignment based on the ICP method is undertaken to improve the registration accuracy.

3.1 Coarse registration

Based on the review of different methods, we propose a novel automated coarse registration method by combining various techniques. The coarse method process consists of three submodules: (1) obtaining point clouds and pre-processing, in this step; (2) B-spline curve fitting and surface reconstruction; (3) principal axes determination and matching.

3.1.1 Obtaining point clouds and pre-processing

The point-based sensor in our inspection system is a laser sensor based on conoscopic holography. One of the drawbacks of the sensor is its limited working range. Therefore, the best accuracy is achieved when the measured surface lies at the center of the working range. This condition implies that the sensor must maintain a constant standoff with the part's surface. For a complex surface, such as a blade, the measurement process to control this constant standoff is challenging. Ref. [12] presented a sensor standoff control method called fixtureless sensor standoff control (FSC), which is a CAD-independent method that does not require manual intervention or a fixture. However, using this method to measure all of the complex surfaces is time-consuming. According to the blade design principle, an improved FSC method is presented here to acquire sufficient points to perform computational registration. Figure 2 shows the schematic diagram of the improved method.

As illustrated in the flowchart of Fig. 2, the single-section line scanning process consists of the following steps: (1) part and sensor position adjustment, (2) linear scan measurement, (3) curve fitting of the scanning path for the next measurement, (4) evaluation, and (5) final scanning for this section line. Then, part and sensor position adjustment is performed according to the twist angle of the blade for the next section line measurement. This procedure is cycled continuously until the last section line is scanned. The single-section line scanning process is described in more detail through the following steps:

Step 1. Part and sensor position adjustment

In a complex surface measurement process, the direction of control for standoff is the z-direction, and the sensor motion in the x- and y-directions is assumed to be a raster motion as shown in Fig. 3a. In other words, the sensor generates equidistant contours in the y-direction on the surface of the part. As shown in Fig. 3b, o_s is the center of the working range of the point sensor. The distance between the sensor and point o_s is designated z_s, which represents the standoff distance of the sensor. Assume that the depth of field of the sensor is 2δ; then, the working range of the sensor can be expressed as $(z_s - \delta, z_s + \delta)$. To obtain additional points for the next step, the relative position of the sensor and part should be adjusted. The starting and ending position should avoid high curvature regions and be as near as possible to the intersection point of a leading/trailing edge with the pressure surface, e.g., the points $p_1$and p_2 shown in Fig. 3b.

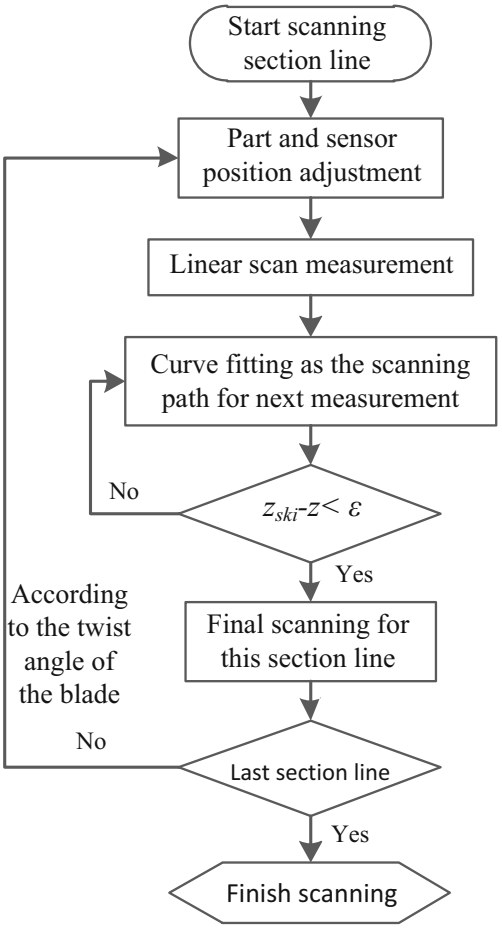

Fig. 2 Schematic diagram of the improved method

Step 2. Linear scanning measurement

The purpose of this step is to obtain sufficient points on the fitting curve as the scanning path for more accurate measurement. In this step, only part of the points that are in the working range will be obtained in the section line, e.g., the red square points in Fig. 3b.

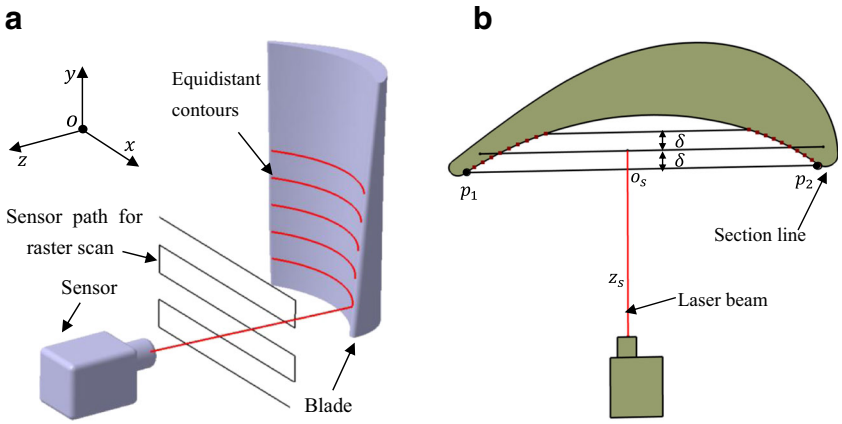

Fig. 3 Sketch map of measurement path of point-based sensors

Step 3. Curve fitting the scanning path for the next measurement

This step uses the points obtained in step 2 to fit a curve as the scanning path for the next scanning, which ensures additional regions in the standoff and captures additional accurate points. Many candidate fitting methods exist, such as B-spline, polynomial, and Bezier, among other methods. Typically, the profile of the turbine blade is of low order (linear or quadratic), and modeling a low-order curve to high order leads to large approximation errors [10]. Using the curve-fitting speed and error, which are two critical issues to ensure dynamic path planning to improve the scanning speed and the surface constructed accuracy, the cubic uniform B-spline is selected to fit the valid data points with curves. The details are introduced in the next section (Section 3.1.2, B-spline curve fitting and surface reconstruction).

Step 4. Evaluation

The coordinates of the surface as measured at a certain measurement step k are (x_{ki}, z_{ki}), and the position of the sensor is (x_{ski}, z_{ski}). Note that the x-coordinate of the sensor is the same as the x-coordinate of the surface for a given measurement step. The sensor positioning error, which is the distance between the actual surface and the estimated measurement, is given by ($z_{ski} - z_s$) for the kth measurement step. z_s is a constant provided by the manufacturer for different lenses of the sensor (e.g., when using the 50-mm lens, the distance $z_s = 44$ mm). The measurement will stop when $|z_{ski} - z_s| \le \varepsilon$, where ε is the predefined threshold, in order to improve the measurement accuracy, ε is set to 1/4 of the depth field of the sensor (e.g., when using the 50-mm lens, the depth of field is ±8mm).

Step 5. Final scanning for this section line

As shown in Fig. 2, during the repetition of step 4, if there is no point recorded by the sensor after it finishes scanning the l_k output of the predefined threshold ε, then l_k is considered the last measured line of this section, and the section line digitization task is completed. The measurement section line has enough points for fitting an accurate curve for the next surface reconstruction step, because the sensor sample frequency can be reached 9000 points/s.

After single-section line scanning is finished, the measured blade angle will be adjusted for the twist angle to complete the next section line, and then steps 1–5 are repeated. When all section line scanning is completed, all point clouds have been obtained for coarse registration.

3.1.2 B-spline curve fitting and surface reconstruction

Point cloud scanning of the suction and pressure side of the blade is conducted to fit the curve and reconstruct the surface for coarse registration.

1. B-spline curve fitting

Considering the curve-fitting speed, which is a critical issue to ensure repetitive path planning, a cubic B-spline fitting algorithm is selected to fit the valid data points with curves. The mathematical formula of the cubic B-spline curve function is

$$C(t) = \sum_{i=0}^{n} B_i N_{i,p}(t) \quad \left(t_{p-1} \le t \le t_{m+1}\right) \tag{1}$$

where B_i are the control points, and $N_{i,k}$ are the normalized B-spline basis functions of order p defined on a knot vector $T = \{t_0, t_1, \ldots, t_{m+p-1}, t_{m+p}\}$.

The process of B-spline curve fitting based on previous measurement points is repeated until the current section line meets the predefined threshold. The fitted B-spline curve is considered the digital contour of the measured section line.

2. Suction and pressure of blade surface reconstruction

Typically, a blade model is reconstructed by a surface lofting operation, also known as skinning, a process passing

a smooth surface through a set of cross-sectional curves [30]. In this study, based on the fitting curves, a surface interpolating all of the curves is considered, with the result that these curves become iso-parametric curves on the lofted surface. B-spline surface lofting is defined as follows [31]:

$$C_k(u) = S\left(u, \bar{v}_k\right) = \sum_{i=0}^{m} \left\{ \sum_{j=0}^{n} v_{i,j} M_{j,q}\left(\bar{v}_k\right) \right\} N_{i,p}(u)$$
$$= \sum_{i=0}^{m} B_{i,k} N_{i,p}(u) \quad (k = 0, \ldots, n) \tag{2}$$

where the (m + 1) points $B_{i,\,k}(i = 0, \ldots, m)$ build up the B-spline control polygon of the kth B-spline curve $C_k(u)$. All $C_k(u)$ curves are assumed to be u-parameter curves of a B-spline surface $S(u, v)$. These curves must be made compatible beforehand, i.e., they must be defined on the same knot vector U with a common order p of B-splines.

For the suction and pressure blade surface reconstruction, the measured points are first used to construct the B-spline interpolation curve and then extended into the B-spline interpolation surface. The deviation between the theoretical surface and the B-spline interpolation surface is calculated as the shape error. In reverse engineering, the shape error is significant; however, the surface fitting in this study uses only coarse registration, as the fitting speed is more important than the accuracy. The purpose of surface reconstruction is to get more and relatively accurate data, which saves a lot of time than using point sensor to get the same data. In practice, according to the design principle of blade, four or five curves are enough to reconstruct the surface that meets the requirement of coarse registration.

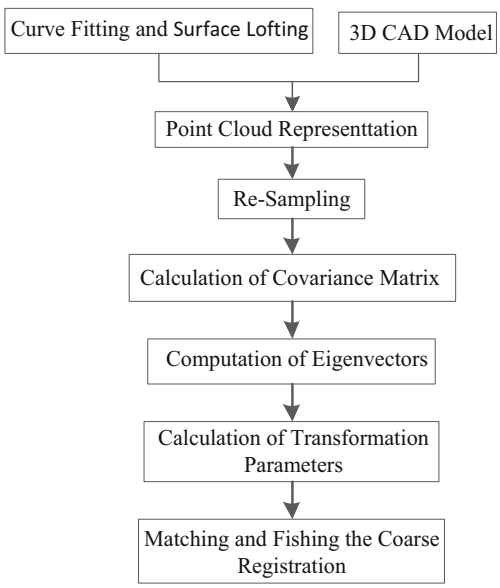

Fig. 4 Overall flow of the proposed coarse registration process

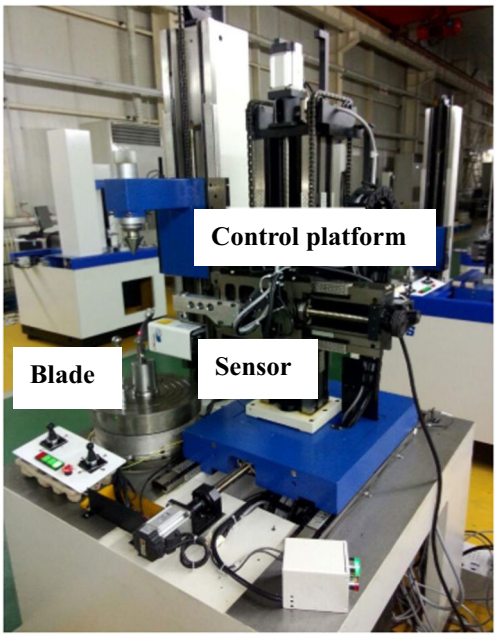

Fig. 5 Four-axis inspection system

3.1.3 Principal axes determination and matching

The use of the principal axes of the object, which contain information on its orientation and position, is the simplest and most widely accepted way to obtain an initial estimate of the 3D data and the CAD model [32]. Principal component analysis (PCA) is the most commonly used technique to determine the principal axes of the two data sets. The basic idea of PCA is to seek a projection that best represents the data in a least-squares sense. Given a 3D data set, the principal axes are defined as the three eigenvectors of the covariance matrix A, which is defined as follows [33]:

$$A = \frac{1}{n} \sum_{i=1}^{n} \left\{ \left(p_i - \overline{p}\right) \left(p_i - \overline{p}\right)^T \right\} \quad i = 1, 2, \ldots, n \tag{3}$$

Table 1 Sensor and coordinate axis parameters list

Names	Specifications
Model	ConoProbe Mark 10.0
Focal length	50 mm
Accuracy	< 6 μm
Resolution	< 0.1 μm
Repeatability	< 1 μm
Laser beam diameter	26 μm
Measuring range	± 8 mm
Distance from the part	44 mm
Scanning speed	9000 points/s
Angle measurement	170°

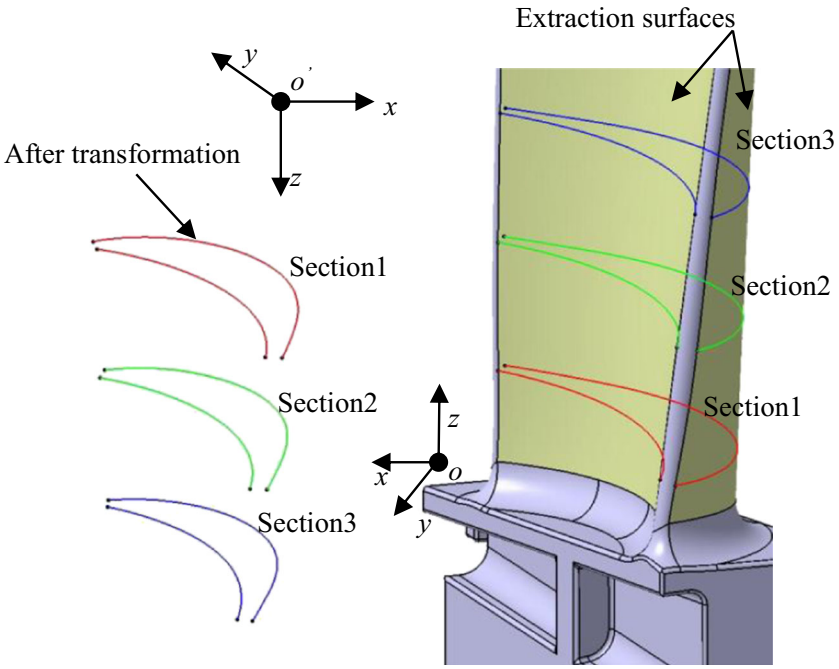

Fig. 6 Process of extraction and coordinate transformation

where n is the number of points in the point set, p_i is the ith point, and $\overline{p}$ is the mean of the n points.

The eigenvector corresponding to the largest eigenvalue of the covariance matrix A is the first principal axis e. A robust technique for determining the principal axes of a 3D shape represented by a point set is presented [32]. The algorithm uses LMS optimization and octree to accelerate computation, an approach that is simple and effective and provides satisfactory results for point-based shapes. (The details are not presented here.) Using the method presented in Ref. [34], the principal axes identification and matching process is shown in Fig. 4.

The present coarse registration method works well where the overlapping sections are almost complete and the objects present no symmetries. During scanning, the cross-section line must approach the top and root of the blade as much as possible. When the suction or pressure blade surface is not complex and exhibits little symmetry, the use of the principal axes to direct the orientation will be unstable. In this case, the suction and pressure surfaces should be scanned at the same time and reconstructed for coarse registration. If the measurement surface of the blade is a long and narrow patch, then the principal axes will be relatively inaccurate, not much information is involved, and the surface direction cannot be accurately represented. Fortunately, this situation rarely occurs in practice.

3.2 Fine registration

Rough registration based on the principal axes aligns the 3D point set with the 3D CAD model by applying the transformation parameters, which provides the initial estimate of the position derived from the 3D point set with respect to that derived from the 3D CAD model. To obtain more accurate results for precision measurement of a blade, a modified ICP registration algorithm based upon this initial estimate is applied.

In our inspection system, a point laser sensor is used based on conoscopic holography, which is a spatially incoherent-light interferometric technique developed by Sirat and Psaltis in 1985 [35], manufactured by Optimet (Jerusalem, Israel). The sensor has a parameter called the signal-to-noise ratio (SNR), which represents the overlap of the fringe frequency from the received laser beams. The SNR value accompanies each individual point and provides a confidence value by which weights can be assigned. The greater this value, the higher the accuracy

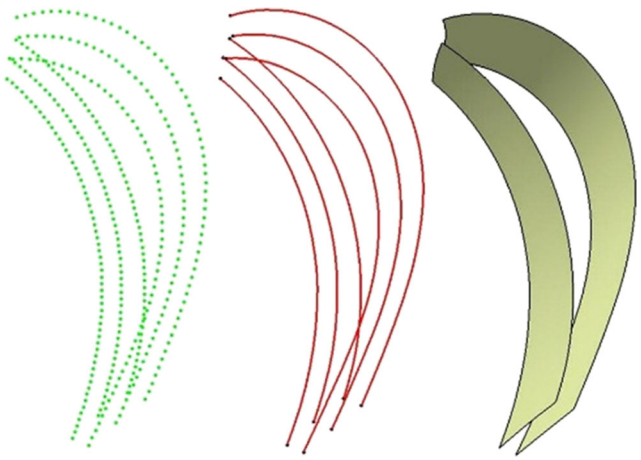

Fig. 7 The results of the curve and surface reconstruction

of the measurement point. A fast ICP registration method using the unit quaternion with an additional weight factor derived from the sensor's SNR was presented in Ref. [27]. The objective is to minimize the following function:

$$\sum_{i=1}^{n} \mathrm{SNR}_i . \left\| p_i - Q^R q_i - Q^T \right\|^2$$

where n is the number of the correspondent pairs, and p_i is the corresponding closest point of the measurement q_i on the design model with the signal-to-noise ratio SNR_i. $Q^R$is the rotation unit quaternion, and $Q^T$is the transition vector.

The registration problem during the blade section line precision inspection is important because it emphasizes aligning the measurement point set with the part model as accurately as possible. To obtain more accurate results, more points in the suction or pressure blade surface must be captured after coarse registration and taking SNR as the weight to optimize. It will be reduced greatly the measurement accuracy impact on the registration method.

4 Development of the four-axis inspection system and experimental validation

In this study, a four-axis inspection system for turbine blades was developed, as shown in Fig. 5. Three linear stages are adopted to provide x, y, and z movements, and a rotary axis is used to orient the part for different views. The sensor used is the Conoprobe fabricated by Optimet, which is attached to the linear stage system. The x- and y-coordinates of a point on the blade surface are recorded directly from the x- and y-axis position of the stages. The z-coordinate on the surface is obtained by adding the z-axis position of the stages to the sensor measurement. The sensor parameters are shown in Table 1. The proposed registration method was implemented on the four-axis system to verify the performance. First, a simulation test was implemented to present a known surface to assess the error of the registration algorithm. Second, the registration method was implemented on the four-axis system to measure the pressure and suction faces of a turbine blade. Finally, the same cross section of the turbine blade was measured by the high-precision CMM and our four-axis inspection system. The measurement data from the CMM and our inspection system were compared and analyzed to verify the correctness of the proposed registration method.

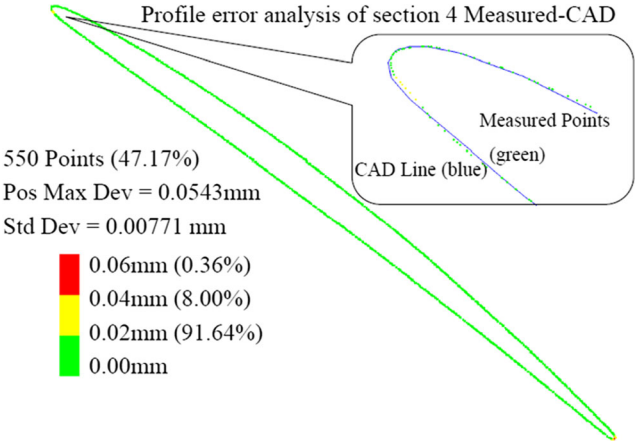

Fig. 9 Comparison of results using our system

4.1 Simulation

To assess the error of the registration algorithm, a simulation program was established to mimic the part measurements with inspection errors. The surfaces used in the simulation were extracted from the CAD model of blades and then transformed to another coordinate system through rotation and translation. The specific process is shown in Fig. 6. Three section lines are obtained from the original design drawing, and the measurement errors ($e \in [-0.006, +0.006]$) are introduced by a random function for simulating the measurement uncertainty. To make

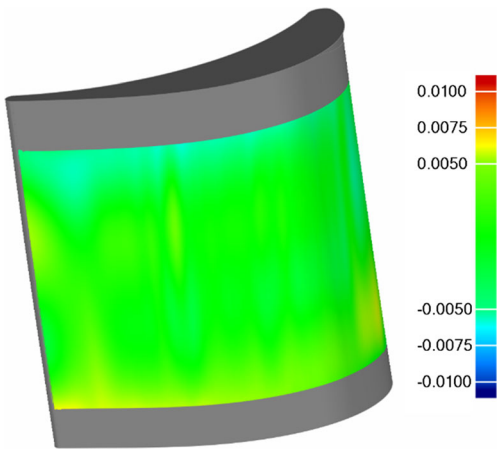

Fig. 8 The comparison results of the curve and surface reconstruction

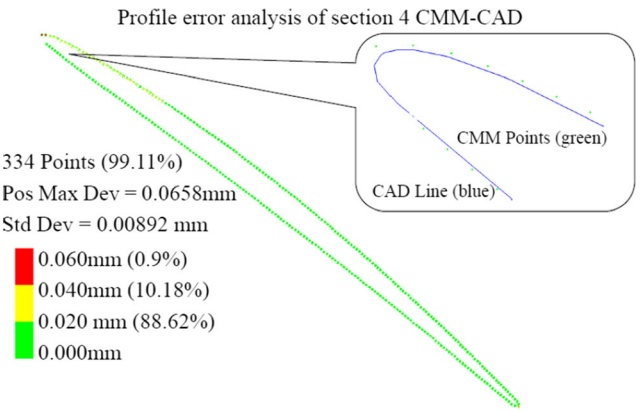

Fig. 10 Comparison of results using the CMM

Table 2 Profile error analysis of section inspection by our system and the CMM

	Points		Max. dev. (mm)		RMS (mm)		< 0.02 percentage (%)	
Section	Measured	CMM	Measured	CMM	Measured	CMM	Measured	CMM
1	500	336	0.0684	0.0777	0.0153	0.0160	40.40	44.35
2	498	336	0.0416	0.0507	0.0098	0.0173	87.15	85.71
3	516	337	0.0874	0.0961	0.0183	0.0145	46.51	48.02
4	550	334	0.0543	0.0658	0.0077	0.0089	91.64	88.62
5	544	332	0.0746	0.0791	0.0164	0.0138	35.66	40.01

the simulation as realistic as possible, the error size of e is selected close to the uncertainty of a real sensor. The simulation provides a virtual test-bed environment to generate the measurement point cloud with controllable errors. This capability is not possible in the actual inspection process, in which the acquired measurement includes the part manufacturing error, sensor detection error, and stage position error. However, the simulated measurements can then be used to verify the accuracy, robustness, and effectiveness of the present registration methods.

The results of curve and surface reconstruction are shown in Fig. 7. A much better level of smoothness curve and surface can be obtained by the present method, which uses the surface to calculate the principal axes to achieve coarse registration and then uses the improved ICP method to complete fine registration to obtain the optimization transformation matrix. The data sets were transformed using the matrix in the same coordinate system as that of the CAD model. The deviation distance was calculated between the data sets and the CAD model. The points were colored in different grades (from blue and green to red) to reveal the deviated distance. The sign of the distance indicates the location (inside or outside) of the measurement point with respect to the surface. The overall root mean square (RMS) error of the simulated registration is 0.0019 mm with a minimum and maximum deviation of − 0.0053 and 0.006 mm, respectively, as shown in Fig. 8. The simulated registration includes other errors, such as facet approximation and point transformation. However, those errors due to the numerical iterations were essentially negligible. From the simulation results, we can know that the initial value is accurate enough, which can effectively prevent the local optimization problem in fine registration.

4.2 Cross-section measurement and profile error analysis

In this experiment, a machined blade is used to inspect the profile error. The geometric dimensions of the blade are 70 × 50 × 20 mm. During the measurement process, the blade is fixed on a rotating platform to rotate around the rotation axis to acquire the complete set of points in the same section plane; five sections of the blade are selected to be scanned. A comparison of the profile errors of the inspection device and the section curve of the CAD is shown in Fig. 9. The maximum absolute errors of the profile are 0.0543 mm. The percentage of errors at less than 0.02 mm is 91.64, and the RMS error is 0.0077 mm. A comparison of the profile errors of the CMM and the section curve of the CAD is shown in Fig. 10. The maximum absolute errors of the profile and the percentage on this selected section by the CMM are slightly larger than that of our inspection device. The maximum absolute errors are shown in Table 2. All the sections are larger, and in the analysis process, we find that they appear primarily at the trailing or leading edge. This

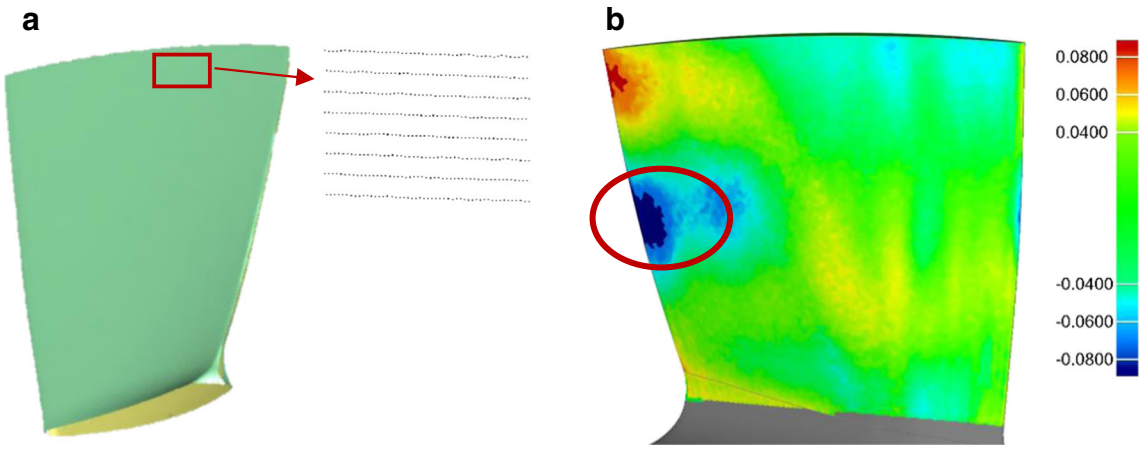

Fig. 11 Case study of the blade inspection by the blade measurement device. (a) Measured point cloud. (b) Error analysis

Table 3 RMS errors of the complete measurement

Deviation range (mm)	Number of points	Percentage (%)
< − 0.08	2085	0.775
− 0.08 to − 0.06	5419	2.013
− 0.06 to − 0.04	14,315	5.318
− 0.04 to 0.04	228,864	85.030
0.04 to 0.06	17,989	6.683
0.06 to 0.08	459	0.171
> 0.08	27	0.010

phenomenon is due to the compensation of the radius of the measuring head or incorrect triggering in the trailing/leading edge measurement process. The optical measuring method does not require radius compensation, and more points can be obtained at the trailing and leading edge, but the CMM offers clear advantages in measuring accuracy.

4.3 A complete measurement of blade and error analysis

In this experiment, the blade is fixed on the rotating platform to rotate around the rotation axis to acquire all points. The pressure, suction surfaces, trailing, and leading edges of the blade were scanned. The distance between every section scanned is 0.1 mm; the points obtained are shown in Fig. 11(a), and the total number of points is 269,158. Such a complete and precise inspection of free-form surfaces is relatively difficult and time-consuming for CMM inspection. The fixture-based industry practice that measures several cross sections of the airfoil would not detect the part errors shown in Fig. 11(b). Table 3 shows that the percentage of deviation in the range of − 0.04 to 0.04 mm is 85.030%. Only 27 points exceed the maximum deviation, and 2085 points exceed the minimum deviation. The RMS error distribution is shown in Fig. 12; most data points exist in the range of − σ to σ, and the percentage lying within the − 3σ to 3σ range is 99.344%.

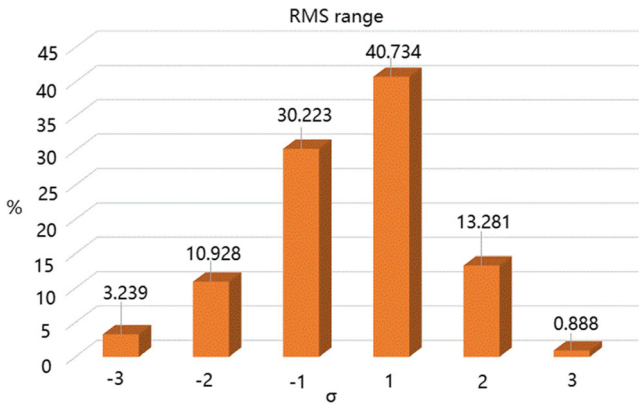

Fig. 12 RMS distribution

5 Conclusion

A robust and accurate automated registration method for turbine blade precision metrology is presented. This method is different from reverse engineering and assess the form quality. The registration in turbine blade precision inspection focuses on unifying the PCS and the MCS to plan the measurement path and find the section curve accurately. Based on the characteristics of the conoscopic holographic sensor and blade surface, an iterative scanning technique is used to acquire sufficient measurements for the reconstruction of the surface, after which the PCA-based method is adopted to complete the initial estimates of the position of the measurement point sets and the CAD model. The results of the coarse registration are refined by the SNR-weighted ICP algorithm. The outliers have little or no effect on the weighted registration process.

The registration method proposed herein was implemented in a four-axis optical blade inspection system. Virtual simulation indicates that the implemented registration algorithm is robust and precise. Section curves and the complete measurement of a turbine blade are measured by the blade inspection system. The experimental results demonstrate that the proposed registration system is a fully automated method for performing the common coordinate system that can be applied to the optical inspection of turbine blades. The complete measurement also reveals part defects that are challenging to detect under current industrial practices.

Funding information This work was funded by National Natural Science Foundation of China (grant nos. 51505134, 51405138, and 51675165) and the University Nursing Program for Young Scholars with Creative Talents in Heilongjiang Province.

References

1. Harding K (2008) Industrial metrology: engineering precision. Nat Photonics 2:667–669. https://doi.org/10.1038/nphoton.2008.218
2. Ross J, Harding K, Hogarth E (2011) Challenges faced in applying 3D noncontact metrology to turbine engine blade inspection. Dimensional Optical Metrology and Inspection for Practical Applications: 81330H. doi: https://doi.org/10.1117/12.895477
3. Chang W-T, Su C-H, Guo D-X, Tang GR, Shiou FJ (2013) Automated optical inspection for the runout tolerance of circular saw blades. Int J Adv Manuf Technol 66:565–582. https://doi.org/10.1007/s00170-012-4350-6
4. Harding K (2010) 3D profilometry: next requests from the industrial viewpoint. Optical Metrol Inspection Ind Appl 785513. https://doi.org/10.1117/12.871778
5. Chang H-C, Lin AC (2005) Automatic inspection of turbine blades using a 3-axis CMM together with a 2-axis dividing head. Int J Adv Manuf Technol 26:789–796. https://doi.org/10.1007/s00170-003-1877-6

6. Mansour G (2014) A developed algorithm for simulation of blades to reduce the measurement points and time on coordinate measuring machine (CMM). Measurement 54:51–57. https://doi.org/10.1016/j. measurement.2014.03.046
7. Hsu T-H, Lai J-Y, Ueng W-D (2006) On the development of airfoil section inspection and analysis technique. Int J Adv Manuf Technol 30:129–140. https://doi.org/10.1007/s00170-005-0046-5
8. Berkovic G, Shafir E (2012) Optical methods for distance and displacement measurements. Adv Opt Photonics 4:441. https://doi.org/10.1364/AOP.4.000441
9. Li Y, Gu P (2004) Free-form surface inspection techniques state of the art review. Comput Aided Des 36:1395–1417. https://doi.org/10.1016/j.cad.2004.02.009
10. Huang J, Yuan Y, Wang Z, Qi Z, Xing C, Gao J (2018) A global-to-local registration and error evaluation method of blade profile lines based on parameter priority. Int J Adv Manuf Technol 94:3829–3839. https://doi.org/10.1007/s00170-017-1125-0
11. Wan N, Liu P, Chang Z, Chen ZC (2018) The machining surface localization of free-form blade considering form tolerance. Int J Adv Manuf Technol 95:4469–4483. https://doi.org/10.1007/s00170-017-1495-3
12. Hsu T-H, Lai J-Y, Ueng W-D, Hwang J-Z (2005) An iterative coordinate setup algorithm for airfoil blades inspection. Int J Adv Manuf Technol 26:797–807. https://doi.org/10.1007/s00170-003-2040-0
13. Srivatsan V, Katz R, Dutta D (2006) Fixtureless sensor standoff control for high-precision dimensional inspection of freeform parts. J Manuf Sci Eng 129:172–179. https://doi.org/10.1115/1.2401621
14. Ravishankar S, Dutt HNV, Gurumoorthy B (2010) Automated inspection of aircraft parts using a modified ICP algorithm. Int J Adv Manuf Technol 46:227–236. https://doi.org/10.1007/s00170-009-2067-y
15. Díez Y, Roure F, Lladó X, Salvi J (2015) A qualitative review on 3D coarse registration methods. ACM Comput Surv 47:1–36. https://doi.org/10.1145/2692160
16. Rantoson R, Nouira H, Anwer N, Mehdi-Souzani C (2015) Novel automated methods for coarse and fine registrations of point clouds in high precision metrology. Int J Adv Manuf Technol 81:795–810. https://doi.org/10.1007/s00170-015-7131-1
17. Johnson AE (1997) Spin-images: a representation for 3-D surface matching. In: PhD thesis. Carnegie Mellon University, USA
18. CHUA CS (1997) Point signatures: a new representation for 3D object recognition. Int J Comput Vis 25:63–85
19. Yamany SM (2002) Surface signatures: an orientation independent free-form surface representation scheme for the purpose of objects registration and matching. IEEE Trans Pattern Anal Mach Intell 24:16. https://doi.org/10.1109/TPAMI.2002.1023806
20. Cheung CF, Li HF, Lee WB, To S, Kong LB (2007) An integrated form characterization method for measuring ultra-precision freeform surfaces. Int J Mach Tools Manuf 47:81–91. https://doi.org/10.1016/j.ijmachtools. 2006.02.013
21. Cheung CF, Li H, Kong L, Lee WB, To S (2006) Measuring ultra-precision freeform surfaces using a robust form characterization method. Meas Sci Technol 17:488–494. https://doi.org/10.1088/0957-0233/17/3/S05
22. Li Y, Gu P (2005) Feature-based alignment and comparison between portion and whole of free-form surfaces. CIRP Ann 54:135–138. https://doi.org/10.1016/S0007-8506(07)60067-5
23. Jiang X, Zhang X, Scott PJ (2010) Template matching of freeform surfaces based on orthogonal distance fitting for precision metrology. Meas Sci Technol 21:045101. https://doi.org/10.1088/0957-0233/21/4/045101
24. Ren MJ, Cheung CF, Kong LB, Jiang X (2012) Invariant-feature-pattern-based form characterization for the measurement of ultra-precision freeform surfaces. IEEE Trans Instrum Meas 61:963–973. https://doi.org/10.1109/TIM.2011.2173047
25. Besl P, McKay N (1992) Method for registration of 3-D shapes. Sensor Fusion IV: Control Paradigms and Data Structures International Society for Optics and Photonics:586–607. https://doi.org/10.1117/12.57955
26. Rusinkiewicz S, Levoy M (2001) Efficient variants of the ICP algorithm. IEEE Comput Soc:145–152. https://doi.org/10.1109/IM.2001.924423
27. Zhu L, Barhak J, Srivatsan V, Katz R (2007) Efficient registration for precision inspection of free-form surfaces. Int J Adv Manuf Technol 32:505–515. https://doi.org/10.1007/s00170-005-0370-9
28. Segal A, Haehnel D, Thrun S (2009) Generalized-ICP. In Robotics: science and systems 2
29. Bouaziz S, Tagliasacchi A, Pauly M (2013) Sparse iterative closest point. Comput Graph Forum 32:113–123. https://doi.org/10.1111/cgf.12178
30. Liu J, Zhao J, Yang X, Liu J, Qu X, Wang X (2015) A reconstruction algorithm for blade surface based on less measured points. Int J Aerosp Eng 2015:1–11. https://doi.org/10.1155/2015/431824
31. Park H, Jung HB, Kim K (2004) A new approach for lofted B-spline surface interpolation to serial contours. Int J Adv Manuf Technol 23. https://doi.org/10.1007/s00170-003-1720-0
32. Liu Y-S, Ramani K (2009) Robust principal axes determination for point-based shapes using least median of squares. Comput Aided Des 41:293–305. https://doi.org/10.1016/j.cad.2008.10.012
33. Chung DH, Yun ID, Lee SU (1998) Registration of multiple-range views using the reverse-calibration technique. Pattern Recogn 31:457–464. https://doi.org/10.1016/S0031-3203(97)00063-0
34. Kim C, Son H, Kim C (2013) Fully automated registration of 3D data to a 3D CAD model for project progress monitoring. Autom Constr 35:587–594. https://doi.org/10.1016/j.autcon.2013.01.005
35. Sirat G, Psaltis D (1985) Conoscopic holography. Optics Letters10:4–6